THE JOURNAL OF PHYSICAL CHEMISTRY C

Article

pubs.acs.org/JPCC

Mechanistic Study of Continuous Reactive Aromatic Organothiol Adsorption onto Silver Nanoparticles

Siyam M. Ansar,[†] Ganganath S. Perera,[†] Patricia Gomez,[∥] George Salomon,[†] Erick S. Vasquez,[‡] I-Wei Chu,[§] Shengli Zou,[∥] Charles U. Pittman, Jr.,[†] Keisha B. Walters,[‡] and Dongmao Zhang*[,†]

[†]Department of Chemistry, Mississippi State University, Mississippi State, Mississippi 39762, United States

[‡]Swalm School of Chemical Engineering, Mississippi State University, Mississippi State, Mississippi 39762, United States

[§]Institute for Imaging & Analytical Technologies, Mississippi State University, Mississippi State, Mississippi 39762, United States

[∥]Department of Chemistry, University of Central Florida, Orlando, Florida 32816, United States

Supporting Information

ABSTRACT: Organothiol (R-SH) (OT) adsorption onto silver nanoparticles (AgNPs) in water was studied for a series of aromatic OTs including *p*-methylbenzenethiol (*p*-MBT), *p*-benzenedithiol (*p*-BDT), and 2-mercaptobenzimidazole (2-MBI). Unlike the common view that OT forms monolayer adsorption on AgNPs, we found that these aromatic OTs continuously reacted with AgNPs through formation of RS−Ag complexes until complete OT or AgNP consumption occurred. The RS−Ag complex can remain on the AgNP surface, converting the AgNPs into core−shell structures. The OT adsorption onto AgNPs occurs predominately through reaction with silver oxide present on the AgNP surfaces before the OT addition or formed from environmental oxygen in the presence of OT. The RS−H protons are completely released when both *p*-MBT and 2-MBI reacted with AgNP, Ag_2O, and $AgNO_3$. However, a substantial fraction of S−H bonds remained intact when *p*-BDT, the only dithiol used in this work, is adsorbed on AgNPs or reacted independently with Ag_2O and $AgNO_3$. The new insights from this work should be important for understanding OT interaction with AgNPs in water and the SERS spectra of the OT adsorbed onto AgNPs.

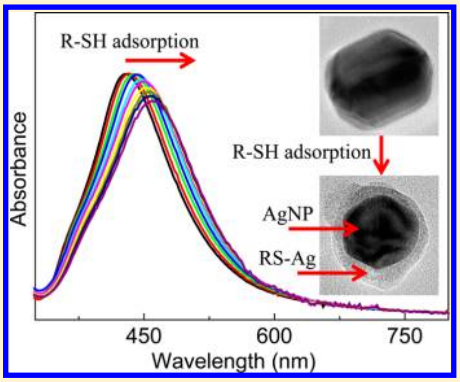

INTRODUCTION

Silver nanoparticles (AgNPs) have been widely used in catalysis, surface-enhanced Raman spectroscopy (SERS), and biosensing and antibacterial applications.[1−7] Organothiol (OT) interactions with AgNPs have been implied in a wide range of AgNP applications where OTs and thiolated biomolecules have been employed extensively for AgNP surface modifications.[8−10] Numerous literature reports are dedicated to the molecular-level OT interfacial interactions with silver surfaces.[11−15] One popular view is that OTs form a monolayer upon adsorption on the silver surfaces, and the properties of the thiol adlayer resemble that of OTs on the gold surfaces.[12,14−18] However, many of these studies were conducted with solid silver films and often with long-chain alkyl OTs dissolved in organic solvents.[14,17,18] The general applicability of the conclusions from these studies of the OT binding to colloidal AgNPs in water under ambient conditions has, to our knowledge, not been systematically examined.

Reported herein is our finding that aromatic OTs can continuously reactively adsorb to the AgNPs in water until complete OT or AgNP consumption takes place. In addition, such spontaneous OT reactive adsorption can convert AgNPs into a structure with a metallic core and a dielectric shell. This observation disagrees with the view that OTs adopt a monolayer adsorption on silver surfaces.[12,15,16,19] Furthermore, our studies indicate that OT adsorption mechanism onto the AgNP in water occurs primarily through Ag_2O on the AgNP surfaces, not by deprotonaton of the SH function as recently proposed.[20−22] The model OTs included in this study are *p*-methylbenzenethiol (*p*-MBT), 2-mercaptobenzimidazole (2-MBI), and *p*-benzenedithiol (*p*-BDT) (Figure 1), and they are chosen for the following reasons. First, these aromatic OTs are commonly used in AgNP-based SERS studies.[23−26] Understanding the mechanism of their interaction with AgNPs may

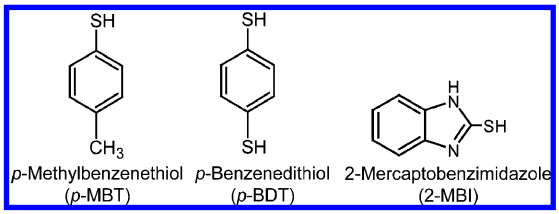

Figure 1. Model organothiols used in this study which include *p*-MBT, *p*-BDT, and 2-MBI.

Received: September 9, 2013
Revised: December 9, 2013
Published: December 9, 2013

   dx.doi.org/10.1021/jp4090102 | J. Phys. Chem. C 2013, 117, 27146−27154

provide new insight into the spectral interpretation. Second, these aromatic OTs are highly UV−vis, Raman, and SERS active, which are important for determining OT structure or concentration on the AgNPs and in solution. Third, the OTs employed here have previously been used to study OT interactions with AuNPs.[11,27−29] Studying the binding of these specific OTs with AgNPs allows us to compare and contrast results to those with AuNPs.

EXPERIMENTAL SECTION

Chemicals and Equipment. All chemicals were purchased from Sigma-Aldrich Inc. except for *p*-BDT, which was purchased from Alfa Aesar, and Ag_2O, which was purchased from Salt Lake Metals. The silver foil (2.5 cm × 2.5 cm × 0.5 mm) and gold foil (2.5 cm × 2.5 cm × 0.127 mm) were purchased from Sigma-Aldrich, and they were used as received. The nanoparticles used in this work include in-house-prepared AgNPs and silver-coated AuNPs (Au@Ag) and commercial AgNPs with a nominal diameter of 50 nm that were purchased from Nanocomposix Inc. (Supporting Information, Figure S1). Nanopure water was used throughout the experiments. The RamChip slides used for the SERS spectral acquisition were obtained from Z&S Tech. LLC. Importantly, the RamChip is a normal Raman substrate that is both fluorescence and Raman background free.[30,31] The SERS spectra were obtained with a Horiba LabRam HR800 confocal Raman microscope system with a 633 nm HeNe Raman excitation laser. UV−vis measurements were taken using a Fisher Scientific Evolution 300 UV−vis spectrophotometer. TEM measurements were made on a Joel 2100.

AgNP Synthesis. The in-house AgNPs were prepared by the Lee−Misel method.[32] Briefly, 0.0282 g of silver nitrate was added to 150 mL of Nanopure water, and the solution was brought to a boil. 3 mL of 1% sodium citrate dehydrate was then added. The solution was kept boiling for another ∼1 h before cooling to room temperature. The surface plasmonic peak absorbance of the as-synthesized AgNPs is at 414 nm. The average particle size of the as-synthesized AgNP is 58 ± 12 nm in diameter, determined by TEM imaging (Supporting Information, Figure S2), and the calculated concentration of the prepared AgNPs was 184.9 pM.

Au@Ag Nanoparticle Synthesis. The gold seeds with diameter of ∼3.5 nm were prepared by the method of Murphy et al.[33] Briefly, 20.0 mL of aqueous solution containing 0.25 mM $HAuCl_4$ and 0.25 mM trisodium citrate was mixed in a conical flask. 0.6 mL of ice-cold, freshly prepared 0.1 M sodium borohydride solution was added dropwise under constant stirring to the $HAuCl_4$/trisodium citrate mixture. The solution was stirred for another 2 h after the complete $NaBH_4$ addition. The Au@Ag particles were prepared by a published procedure with modification.[33] Briefly, 10 mL of 0.32 mM $AgNO_3$ and 20.0 mL of as-synthesized gold seeds were mixed, and the solution was brought to boil for ∼10 min. After the solution cools to room temperature, 1.2 mL of ice-cold, freshly prepared 0.1 M sodium borohydride solution was added dropwise under constant stirring to the Au seed/$AgNO_3$ mixture. The solution was stirred for another 1 h after the complete $NaBH_4$ addition.

OT Adsorption onto AgNPs. Unless specified otherwise, all the OT adsorption experiments were performed with the following procedure. After addition 1.0 mL of three times diluted in-house AgNPs into 2.0 mL of OT solution in a 4.5 mL glass vial, the mixtures were vortexed briefly, then capped, and settled at ambient conditions. The nominal OT concentration in the ligand binding solutions is 50.0 μM. Since 2-MBI and *p*-MBT adsorption induces AgNP aggregation and settlement, the amount of the OT adsorbed onto AgNPs was estimated on the basis of the amount of UV−vis determination of the OT free in the supernatants.

2-MBI Adsorption onto Gold and Silver Foils. The received silver (2.5 cm × 2.5 cm × 0.5 mm) and gold (2.5 cm × 2.5 cm × 0.127 mm) foils were cut into small squares with dimensiona of ∼0.5 cm × ∼0.5 cm. After placing the silver and gold squares at the bottom of two separate 4.5 mL UV−vis cuvettes, 2 mL of 17.5 μM 2-MBI solution was added into each cuvette. The time courses of 2-MBI adsorption onto the gold and silver foils were monitored by UV−vis quantification of the amount of 2-MBI remaining in the supernatant. The cuvettes were sealed with paraffin to prevent solvent evaporation during the entire experimental period.

SERS Spectrum of OT Adsorbed onto AgNPs. 10 μL of OT solution was mixed with an equal volume of in-house colloidal AgNP solutions. After vortexing for ∼1 min, 10 μL of 1% KCl solution was added to the AgNP/OT mixture as the aggregation agent, and 10 μL of the final solution was transferred to a RamChip slide for SERS spectral acquisition. All the SERS spectra of OT/AgNP were taken with an Olympus 20× objective, grating of 600 grooves/mm, and a laser intensity before reaching sample of 1.3 mW. The spectral integration time varied from 1 to 10 s. The Raman shift was calibrated with a neon lamp, and the Raman shift accuracy was ∼0.5 cm^{-1}. The nominal OT concentration in the AgNP containing samples is ∼30 μM.

OT/Ag Complex. To study the OT structure on AgNPs, we compared the SERS spectra of OT adsorbed onto AgNPs with the normal Raman spectra of the OT/Ag complex prepared by OT reaction with Ag_2O and by OT reaction with $AgNO_3$. The OT/Ag complex by OT reaction with Ag_2O is prepared by overnight shaking 2 mg of Ag_2O mixed with 1.0 mL of ∼20 mM OT in 50% EtOH. The precipitated OT/Ag complex was washed with EtOH and dried under ambient conditions before Raman spectral acquisition. OT/Ag complexation by reacting OT with $AgNO_3$ was conducted as follows. First 10.0 mL of 10 mM of $AgNO_3$ in water was mixed with a vortex mixer with 10.0 mL of ∼10 mM OT in 50% EtOH. After overnight incubation of $AgNO_3$/OT mixture, the OT/Ag complex was washed with EtOH and dried under ambient conditions before Raman acquisitions. To explore the reaction stoichiometry between *p*-BDT, a dithiol, and $AgNO_3$, we also prepared the *p*-BDT/Ag complex by mixing 10.0 mL of 20 or 30 mM $AgNO_3$ in water with 10.0 mL of ∼10 mM *p*-BDT in 50% EtOH.

Normal Raman Spectra of OT and OT/Ag Complex. Normal Raman spectra of OT or the OT/Ag complex were acquired by depositing a flake of as-received OT powder or the above-synthesized OT/Ag complex onto the RamChip slide. All the Raman spectra were taken with an Olympus 20× objective, grating of 600 grooves/mm, and a laser intensity before sample of 1.3 mW. The spectral integration time varied from 5 to 60 s for the samples.

2-MBI Adsorption onto AgNPs in Which the Headspace Was Filled with Air and Nitrogen. 30.0 mL of 2-MBI 100 μM and 30.0 mL of as-synthesized AgNPs were added into each of two 100 mL three-neck round-bottom flasks under constant stirring. The headspace of one flask is filled with a constant flow of air and the other with nitrogen. To determine the amount of 2-MBI adsorption as a function of time, 1.0 mL of the reaction mixtures was removed from the solution at

dx.doi.org/10.1021/jp4090102 | J. Phys. Chem. C 2013, 117, 27146−27154

predefined time period. After centrifugal removal of the AgNPs together with their surface adsorbates, the amount of free 2-MBI (unbounded) in the supernatant from the removed 2-MBI/AgNP mixture was quantified with UV−vis.

Dynamic Light Scattering (DLS). Data were collected using a ZetaPALS instrument (Brookhaven Instruments Corporation). All measurements were conducted at ambient conditions (~20 °C), with a laser wavelength of 659 nm and a 90° angle of detection. All samples were mixed with a vortex mixer for 30 s prior DLS analysis. Samples were then stabilized for 3 min before data collection. A total of five measurements (2 min per measurement) were acquired on each sample for particle size determination. Average results are reported for the mean hydrodynamic diameter obtained by intensity, which was fitted using the non-negative least-squares algorithm. Data were measured and analyzed using Particle Solutions software v2.0 provided by the instrument vendor.

TEM Analysis. The morphological structure of OT-treated AgNP was examined with TEM. Possible free OTs in the OT/AgNP mixtures were removed before TEM measurements. Since 2-MBI and *p*-MBT induced spontaneous AgNP aggregation and settlement, the free OT in the 2-MBI/AgNP and *p*-MBT/AgNP mixtures was removed by simply washing the AgNP precipitates three times with Nanopure water. AgNPs in the *p*-BDT/AgNP mixtures was stable (no aggregation). The removal of free *p*-BDT in *p*-BDT/AgNP mixtures was conducted by centrifugation followed with water washing. TEM images were taken with Cu grids covered with a Formvar carbon film at an accelerating voltage of 200 kV.

Thermogravimetric (TGA) Analysis. The 2-MBI/AgNP sample for TGA was prepared by shaking for 1 week the mixture of 139 mL of as-prepared AgNPs and 27 mL of 1.5 mM 2-MBI in water. The amount of MBI adsorbed onto AgNPs was quantified on the basis of UV−vis measurement of the free MBI in the supernatant. The aggregated AgNPs containing adsorbed 2-MBI were filtered, washed with EtOH, and dried under ambient conditions before TGA analysis. TGA was conducted using a DSC-TGA (SDT Q-600, TA Instruments) under a nitrogen flow (50 mL/min). A minimum sample weight of 5 mg was used for the measurements with a heating rate of 10 °C/min.

Computational Simulations of AgNP LSPR. We calculated the extinction efficiency of AgNPs with different core sizes and shell thickness using the generalized Mie theory.[34,35] In the calculations, the dielectric constants of silver are taken from Palik's handbook.[36] The indices of refraction of the *p*-BDT are taken as 1.67, which was obtained from a *p*-BDT vendor (Santa Cruz Biotechnology, Inc.). The length of the *p*-BDT molecule is set as 0.8 nm, and the van der Waals diameter of the Ag atom is 0.344 nm.[37] When *p*-BDT molecules react with Ag nanoparticles, we calculated extinction spectra at three different conditions. We first removed both Ag atoms and *p*-BDT molecules from the solution. In the second condition, we kept the size of the AgNP unchanged while attaching all the adsorbed *p*-BDT molecules as a shell. In the last condition, the Ag atoms were detached gradually from the AgNPs but they formed a complex with *p*-BDT and attached to the remaining AgNPs as a shell. As shown in Figure S3C, for the first case, the resonance wavelength of the nanoparticle blue-shifts with increasing concentration of added *p*-BDT molecules and the extinction efficiency drops. The resonance wavelength of Ag nanoparticles will red-shift when the AgNP core is unchanged and the adsorbed *p*-BDT molecules are attached to the core to form a core−shell structure. However, the extinction efficiency grows with increasing amounts of adsorbed *p*-BDT molecules (Figure S3A). Only at the last condition, the resonance wavelength red shifts and the extinction efficiency drops when more *p*-BDT molecules are adsorbed (Figure 3C). This agrees with the experimental observation.

RESULTS AND DISCUSSION

Unless specified otherwise, the OT/AgNP binding experiments were conducted with freshly prepared AgNPs (within 1 week). In addition, the OT binding experiments were performed in capped 4.5 mL glass vials at ambient conditions, unless specified otherwise. While 2-MBI and *p*-MBT adsorption induces immediate AgNP aggregation and eventual settlement (Figure 2), the AgNPs in the *p*-BDT-containing solution

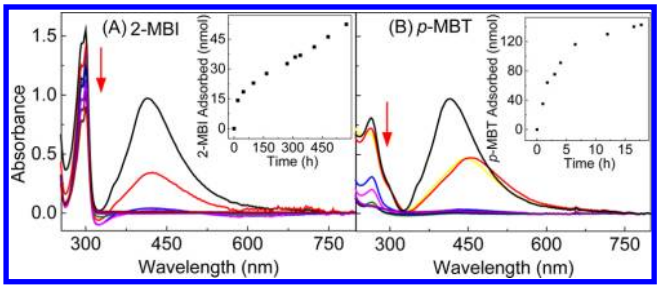

Figure 2. UV−vis spectrum of (A) 2-MBI/AgNP and (B) *p*-MBT/AgNP mixtures as a function of the sample incubation time. The spectrum in black is the in-house AgNP control that is the mathematically additive spectrum of the UV−vis spectrum of in-house AgNP and OT in water. The complete aggregation and precipitation of the AgNPs are shown by the absence of the AgNP localized surface plasmonic resonance (LSPR) peak in the 400 nm region. The inset shows the amount of OT adsorbed onto AgNPs by assuming the UV−vis intensity reduction is exclusively due to OT adsorption onto AgNPs. The nominal OT and AgNP concentrations in the AgNP-containing samples are 50 μM and 20.55 pM, respectively. The arrow indicates the increasing sample incubation times.

remain well-dispersed (Figure 3). The complete AgNP settlement in 2-MBI/AgNP or *p*-MBT/AgNP mixtures was evident from the total absence of AgNP LSPR feature in the UV−vis spectra obtained with their respective solution (Figure 2). The exact reason for the different AgNP aggregation characteristics among these samples is currently unclear but may be related to the fact that there is a significant fraction of the −SH groups in *p*-BDT on AgNPs remains unreacted as it will be shown later in this work. The remaining −SH group could make the *p*-BDT-containing AgNP more water compatible than *p*-MBT- and 2-MBI-containing AgNPs because the distal groups in *p*-MBT and 2-MBI on AgNP are benzene. That is more hydrophobic than the terminal −SH group in *p*-BDT.

The continuous OT adsorption onto the AgNPs was demonstrated in all the samples by the monotonically decreased OT concentration in the supernatant of the ligand binding solutions (Figure 2) and by the reduced *p*-BDT UV−vis absorbance in the time-resolved UV−vis spectra obtained with the *p*-BDT/AgNP mixture (Figure 3A). This continuous OT adsorption onto AgNPs is drastically different from the adsorption of the same OTs onto the AuNPs reported in our recent studies.[11,38] OT reaches steady-state adsorption on AuNPs within the first few minutes of the sample

dx.doi.org/10.1021/jp4090102 | J. Phys. Chem. C 2013, 117, 27146−27154

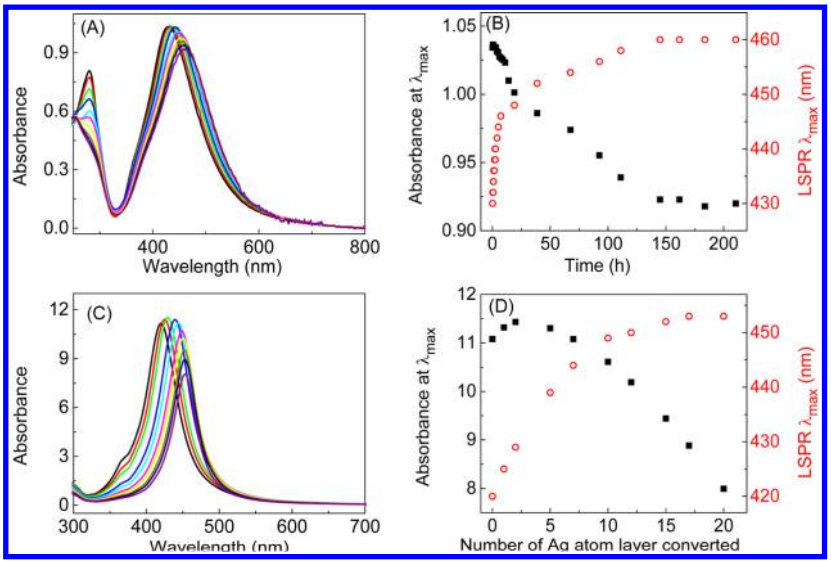

Figure 3. Experimental time-dependent UV−vis spectra of (A) the *p*-BDT/AgNPs and (B) the time course of the in-house AgNP LSPR peak absorbance and peak wavelength as a function of incubation time. (C) Computationally simulated AgNP LSPR spectra in which the surface layer of Ag atoms in AgNPs is progressively converted into *p*-BDT-Ag. (D) Computed AgNP LSPR peak absorbance and peak wavelength as a function of surface Ag atom layers converted to Ag-BDT complexes. The nominal *p*-BDT and AgNP (~58 nm in diameter) concentrations in the AgNP-containing samples are 50 μM, and 20.55 pM, respectively.

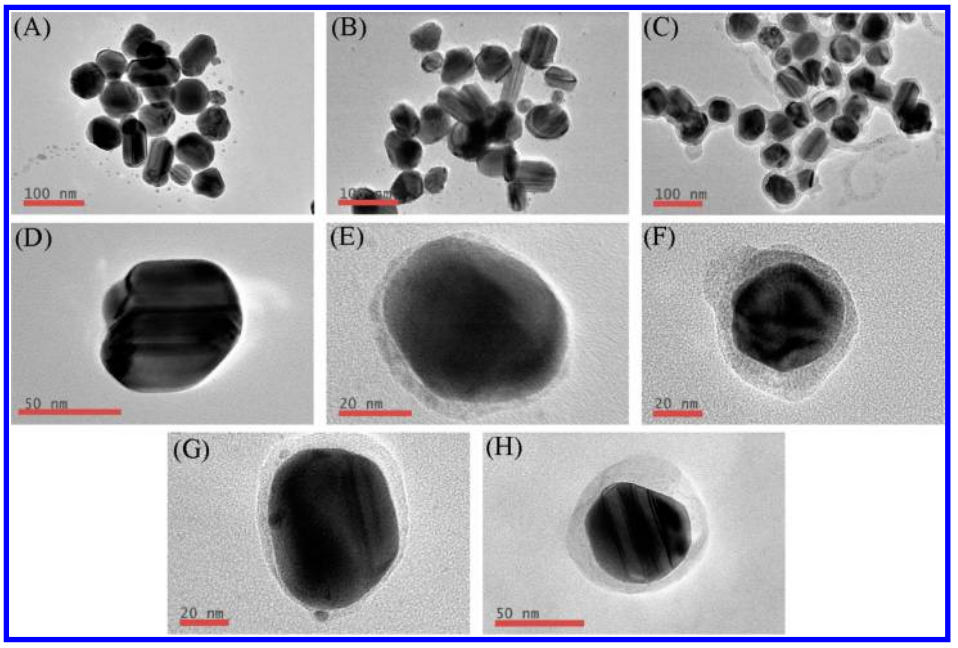

Figure 4. TEM images obtained with (A) as-synthesized AgNPs, (B) AgNPs incubated with 2-MBI for 4 days and (C) 1 month. (D−F) Zoom-in single AgNP TEM images from the samples used for (A−C), respectively. (G, H) AgNPs from *p*-MBT/AgNP and *p*-BDT/AgNP mixtures each incubated 4 days. The nominal OT and AgNP concentrations are 100 μM and 92.5 pM, respectively.

incubations.[11,38] It is important to note that 2-MBI remains totally stable in the control solutions under the experimental conditions (Figure S4). In contrast, *p*-MBT and *p*-BDT have limited stabilities in water solutions containing no AgNPs. Control experiments showed that UV−vis absorbance of these two OTs in water decreases with prolonged incubation (Figure S4). Therefore, the amount of *p*-MBT and *p*-BDT adsorbed onto AgNPs as a function of time depicted in Figures 2 and 3 should only be treated as semiquantitative. Quantitative delineation of the *p*-MBT and *p*-BDT UV−vis absorbance reduction induced by AgNP binding and by OT degradation is currently impossible. Therefore, quantitative ligand adsorption studies were performed with 2-MBI alone.

The amount of the 2-MBI adsorbed onto the AgNPs is more than 23 times higher than the monolayer packing capacity of 2-MBI on the AgNPs that is predicted on the basis of the AgNPs' sizes and concentrations (Supporting Information). TGA conducted with a separately prepared 2-MBI-treated AgNP sample confirms that the 2-MBI depleted from the ligand binding solution had coprecipitated with AgNPs (Figure S5). Detailed TGA experimental results obtained with the 2-MBI/AgNP mixture, the 2-MBI powder, and Ag_2O are shown in Figure S5. The experimental weight loss of MBI-treated AgNPs

dx.doi.org/10.1021/jp4090102 | J. Phys. Chem. C 2013, 117, 27146−27154

(12%) is in agreement with the weight percentage (14%) of 2-MBI adsorbed onto the AgNPs. This quantity was deduced by UV−vis quantification of 2-MBI depleted from the supernatant in the 2-MBI/AgNP mixture. The small difference between the TGA result and that deduced from UV−vis measurement is probably due to some of adsorbed 2-MBI that was lost in the ethanol wash and filtering (Figure S5).

Transmission electron microscopic (TEM) analyses obtained with the precipitates in the 2-MBI/AgNP mixtures showed that all the AgNPs were converted to core−shell structures with shell thicknesses increasing with more 2-MBI adsorbed (Figure 4, A to C and D to F). Similar core−shell structures were also observed in TEM images of AgNPs mixed with *p*-MBT or *p*-BDT (Figure 4, G and H). The largest shell thickness observed on AgNPs in the 1-month-aged 2-MBI/AgNP mixture is ∼10 nm, which is significantly larger than the 2-MBI molecular dimensions. Importantly, similar core−shell structures are also observed in the TEM images obtained with the commercial 50 nm AgNPs treated with all the model OTs (Figure S6). The AgNP core size of the commercial AgNPs was calculated for AgNPs with and without *p*-BDT mixed. The average diameter of the as-received AgNPs is 48.1 ± 2.8 nm, which was reduced to 40.6 ± 4.9 nm after incubating with *p*-BDT for 10 days. The average shell thickness in the *p*-BDT-treated AgNPs is 17 ± 7.5 nm (Figure S7). This is calculated by assuming that the AgNPs were uniformly coated.

Further confirmation of the AgNP core−shell formation comes from the DLS measurements conducted for the commercial 50 nm AgNPs mixed *p*-BDT in which the AgNPs are stable in solution (no aggregation). The DLS hydrodynamic diameter of the as-received AgNPs is 52 ± 1 nm, while diameters of the *p*-BDT covered AgNPs increased to 78 ± 3 and 89 ± 2 nm in an equal volume mixture of 100 μM *p*-BDT and the as-received AgNP that is aged for 1 h and 3 days, respectively (Table S1). Evidently this increment in the AgNP diameter far exceeds the height of monolayer *p*-BDT. The length of *p*-BDT is ∼0.8 nm.[37] This DLS result that was directly obtained with the *p*-BDT/AgNP mixture. It indicates that the coating on the AgNP surfaces observed in the TEM image of the aromatic OT-treated AgNPs are formed in solution, not during the TEM sample preparation. Importantly, excess OT was removed before loading the OT-treated AgNPs onto the TEM grid. This was described in the Experimental Section.

The only sensible explanation for the appearance of this coating is that OTs progressively react with and convert the AgNP surface silver atoms into OT/Ag complexes. At least some of the RS−Ag complexes remain attached to AgNPs. We indeed observed a relative small amount of amorphous precipitate that separated from the AgNPs in the month-old AgNP/2-MBI mixture (Figure 4C). These amorphous precipitates are likely OT/Ag complexes formed by AgNP surface atoms etched away by the OTs. They may also be the OT/Ag complexes detached from AgNP core in our TEM sample preparation. Regardless, irregularity of the shell and presence of isolated precipitates limit our ability to quantitatively study to correlation between shell thickness and the amount of 2-MBI adsorbed. However, most of the 2-MBI−Ag complex retained on the AgNPs in the AgNP/OT mixture was aged for 4 days. Comparison of the TEM images and energy dispersive spectroscopy (EDS) obtained with AgNP/2-MBI mixture confirms sulfur is present in both AgNPs and the amorphous precipitates (Figure S8). Unfortunately, the EDS resolution of our TEM (Jeol 2010) instrument is not high enough for elemental mapping of the coating layer on the AgNPs.

The time-resolved UV−vis spectra obtained with AgNP/*p*-BDT mixtures (Figure 3) are consistent with our explanation for the continuous reactive OT adsorption onto AgNPs and our DLS results obtained with the AgNP/*p*-BDT mixture. The AgNP LSPR peak absorbance is monotonically reduced, and its peak wavelength is red-shifted as a function of continuous *p*-BDT adsorption. Computational simulation confirms that the *p*-BDT-Ag dielectric layer thickness keeps increasing and the AgNP core diameter keeps decreasing. This is the only possible way for red-shifting to occur in the AgNP LSPR peak wavelength along with a simultaneous monotonic decrease of the AgNP LSPR peak absorbance (Figure 3C). The AgNP LSPR peak absorbance would increase monotonically if the *p*-BDT shell thickness increases, but the size of the AgNP core does not change (Figure S3). In contrast, the blue-shift in the AgNP LSPR peak wavelength would be observed if *p*-BDT converts surface Ag atoms into *p*-BDT/Ag complexes, but these complexes are not retained on the AgNPs (Figure S3).

Definitive proof of the continuous reactive OT interaction with AgNPs came from a comparative study of 2-MBI adsorption onto gold-core−silver-shell (Au@Ag) bimetallic nanoparticles and AuNP seeds in which the amount of AuNP seeds is kept constant (Figure 5). Au@Ag nanoparticles were prepared using the procedure of Murphy et al. with modifications (Figure S9).[33] The 2-MBI adsorption onto the AuNP seeds rapidly reached a steady state. However, the amount of 2-MBI depleted from the supernatant in the 2-MBI/Au@Ag mixture keeps increasing until the difference in the amount of the 2-MBI adsorbed by Au@Ag versus AuNP seeds equals the amount of the silver atoms present in the Au@Ag. This experiment proved that 2-MBI reacted quantitatively with all the Ag atoms presented in Au@Ag and confirmed that one 2-MBI molecule reacted with each Ag atom. This stoichiometry is consistent with the reported stoichiometric ratio found when a monoalkanethiol reacts with Ag^+.[39,40]

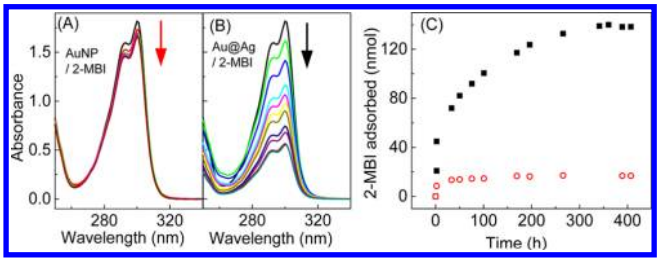

Figure 5. UV−vis spectra obtained of the supernatant in (A) 2-MBI/AuNP and (B) 2-MBI/Au@Ag mixtures as a function of sample incubation time. The arrow indicates the increasing sample incubation times. (C) Comparison of 2-MBI adsorption onto (○) AuNP seeds and (■) Au@Ag nanoparticles as a function of the sample incubation time. The total amount of silver atoms coated onto the AuNP seeds in the Au@Ag nanoparticles used in (B) is 103 nmol, which is calculated by assuming that all the Ag^+ added onto the Au seed is reduced.

Combining both pH and SERS measurements indicates that the OT interaction with AgNPs is predominantly due to an OT reaction with the Ag_2O known to be on the AgNP surfaces.[41−43] Moreover, it rules out the possibility that OT reaction with Ag^+ or zero valence Ag(0) atoms is the dominant pathway governing the OT binding to AgNP surfaces. The

dx.doi.org/10.1021/jp4090102 | J. Phys. Chem. C 2013, 117, 27146−27154

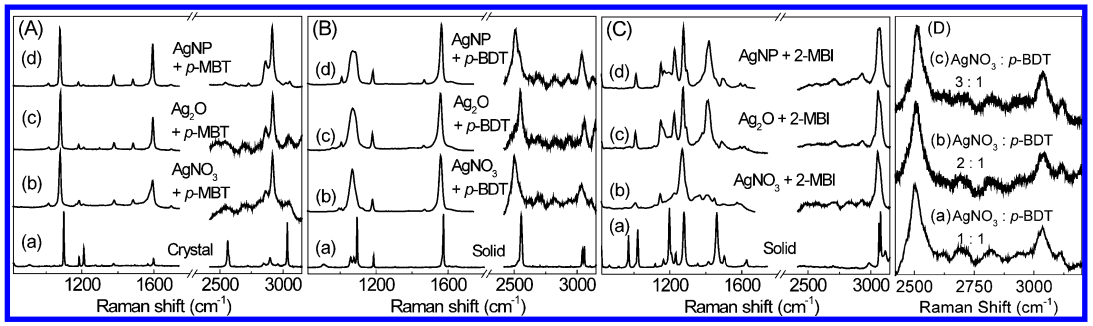

Figure 6. Raman spectra obtained of (A) *p*-MBT, (B) *p*-BDT, and (C) 2-MBI: (a) solid OT, (b) OT/Ag complex obtained by an OT reaction with equivalent amount of $AgNO_3$, and (c) Ag_2O, (d) OT adsorbed onto AgNPs. Detailed procedures used are described in the Experimental Section. (D) Raman spectrum of *p*-BDT/Ag complex formed by mixing *p*-BDT and $AgNO_3$ of molar ratio of (a) 1:1, (b) 1:2, and (c) 1:3. The spectra were offset and scaled for clarity.

SERS spectra of the OT adsorbed onto the AgNPs are highly similar to normal Raman spectra of the products of OT reaction with either Ag_2O or Ag^+, but different from normal OT Raman spectra (Figure 6). Previous literature showed that aqueous 2-MBI is in the thione tautomeric form, but in the thiolate form on the AuNPs.[28] The complete absence of the S−H Raman spectral feature in the 2600 cm^{-1} region in *p*-MBT and 2-MBI SERS and also their Ag complexes indicates the −SH hydrogen atom has been released in each case. This might occur through one or more of the pathways depicted in eqs 1−4 in Figure 7. However, the first three of these possible

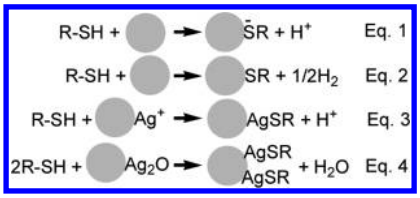

Figure 7. Possible reaction pathways for OT adsorption onto AgNPs. Ag^+ and Ag_2O refer to possible silver ion and silver oxide on AgNP surface, respectively.

pathways were excluded on the basis of control experiments. They showed no pH change or hydrogen gas generation occurs when OT is adsorbed onto AgNPs (Figure S10). In contrast, OT reaction with Ag^+ (in $AgNO_3$) releases thiol protons and reduces solution pH (Table S2). The reaction pathways depicted by eqs 1 and 2 would lead to pH reduction or hydrogen generation, respectively, when OT binds to AgNPs. However, eq 4 leads to no pH changes, which was also confirmed by control experiments that showed no pH change when Ag_2O powder was added into OT solutions (Figure S11). We recently demonstrated that OT adsorption onto AuNPs in water reduces solution pH, and the amount of the protons released from OTs was linearly correlated to the amount of OT adsorbed.[11] These pH measurements highlight the difference in the fundamental mechanism between OT binding onto AgNPs and AuNPs in water. The OT interaction with AuNPs involves the deprotonation of R−SH, while the OT interaction with AgNPs is primarily due to the reaction of R−SH with Ag_2O formed on the AgNP surface.[41−43] Henglein reported that AgNPs are extremely sensitive to environmental oxygen.[44] Exposing AgNPs synthesized under argon protection to ambient air as short as 1.5 min induces substantial change in the AgNP LSPR. This change is due to the AgNP surface atom oxidation.[44] Since the commonly used citrate-reduced AgNPs are normally prepared and stored with no inert gas protection or solution purging, it is reasonable that surface Ag atoms are oxidized soon after the AgNP preparation.

Notably, the SERS spectra in Figure 6 show that not all the −SH hydrogen atoms are released in any of the *p*-BDT reaction products with $AgNO_3$, Ag_2O, or AgNPs. Indeed, a substantial S−H stretch feature (~2500 cm^{-1}) appeared in the SERS spectrum obtained with *p*-BDT adsorbed on AgNPs and in the Raman spectra of the *p*-BDT/Ag complexes obtained by *p*-BDT reaction with Ag_2O or Ag^+. This remained true for the *p*-BDT/Ag complexes formed by mixing $AgNO_3$ and *p*-BDT with an $AgNO_3$/*p*-BDT concentration ratio of 3:1 (Figure 6D). These data strongly suggest that only one −SH in *p*-BDT reacted with AgNP, Ag_2O, or Ag^+ under our experimental conditions. This result is consistent with our recent pH titration experiment that reveals that the pK_as of the two SH groups in *p*-BDT differ by at least 7 pK_a units both in *p*-BDT solutions

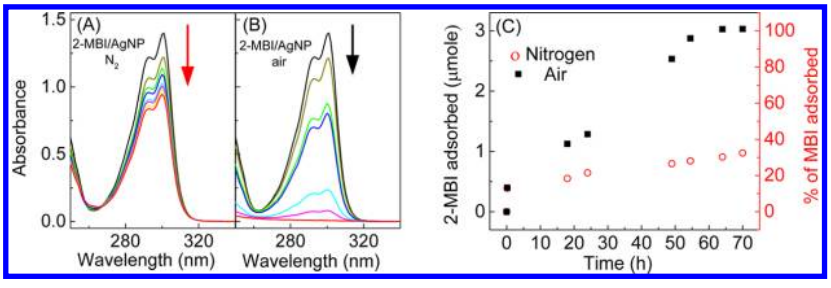

Figure 8. (A) UV−vis spectra obtained with the supernatants of the (A) the nitrogen-filled and (B) air-filled 2-MBI/AgNP mixtures as a function of the sample incubation times. (C) The amount of 2-MBI adsorbed onto the AgNPs as a function of the sample incubation time for (○) nitrogen- and (■) air-filled 2-MBI/AgNP mixtures in (A) and (B). Experimental details are described in the Supporting Information. The nominal 2-MBI and AgNP concentrations in the samples are 50 μM and 20.55 pM, respectively.

dx.doi.org/10.1021/jp4090102 | J. Phys. Chem. C 2013, 117, 27146−27154

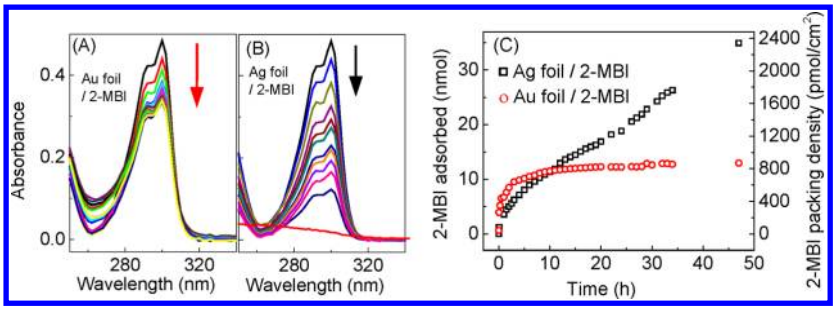

Figure 9. (A) Representative UV−vis spectra obtained with (A) Au foil/2-MBI and (B) Ag foil/2-MBI mixtures as a function of the sample incubation time. (C) The amount of 2-MBI adsorbed onto the metal foils and nominal 2-MBI packing density on the foil as a function of the sample incubation time for (○) Au foil/2-MBI and (□) Ag foil/2-MBI mixtures in (A) and (B). The initial 2-MBI concentration is 17.5 μM in both samples. Arrows in (A) and (B) indicate increasing sample incubation time. Complete 2-MBI adsorption onto Ag foil is evident from the absence of the 2-MBI UV−vis absorption in the UV−vis spectrum obtained with the 2 day incubated Ag foil/2-MBI sample. Experiment details are described in the Experimental Section.

and for *p*-BDT on AuNPs.[11] On the other hand, these data disagree with the previous reports that both thiols in *p*-BDT are deprotonated on AuNP and AgNPs.[24,29]

The presence of this S−H stretching feature also excluded the possibility that the coating layer on the *p*-BDT-treated AgNP is polydisulfurized *p*-BDT $-(S-C_6H_4-S)_n-$. Polydisulfide would not have significant S−H stretch in the SERS obtained with the *p*-BDT treated AgNPs. Indeed, detectable disulfide formation can also excluded on the basis of the Raman and SERS spectra of the OT and OT/AgNP complexes obtained in the Raman shift region from 250 to 1650 cm^{-1} (Figure S12). Diphenyl disulfide has a strong S−S stretch at 524 cm^{-1}.[45,46] The complete absence of a S−S signal in the OT/AgNP SERS spectra indicates that there is no significant disulfide formation in the OT adsorbed onto AgNPs in any of the samples.

The OT reaction with AgNPs in water via the silver oxide pathway described above disagrees with the view that OT adsorption onto AgNPs involves the deprotonation of the thiol proton in the OTs.[20,21,47] A reactive adsorption mechanism through Ag_2O is also supported by additional 2-MBI binding experiments that were conducted in two different reaction vessels, where the headspace was filled with a constant flow of either air or nitrogen (Figure 8). During an experimental period of 2 days, the 2-MBI added into the air-filled aqueous AgNP suspension was totally depleted from the supernatant, and the amount of 2-MBI adsorbed onto AgNPs onto the air-filled sample is 3.4 times higher than the 2-MBI reacted with AgNPs in the nitrogen-filled sample. Complete 2-MBI disappearance was demonstrated by the absence of any 2-MBI UV−vis spectral feature in the supernatant from the AgNP/2-MBI mixture (Figure 8B). Importantly, no significant pH changes occurred in either of the solutions. This excludes the possibility of 2-MBI reactions with Ag^+ and Ag(0). In other words, the 2-MBI interactions with both the nitrogen- and air-filled AgNPs in water must predominately follow the silver oxide pathway.

The time courses of 2-MBI adsorption onto AgNPs depicted in Figure 8 are consistent with the literature reports that as-synthesized AgNPs in water are coated with Ag_2O.[41−43] The most plausible explanation for the rapid and mostly identical initial 2-MBI loss from the supernatant solutions in both the air- and nitrogen-filled AgNP samples is that the AgNP surface atoms have been oxidized to Ag_2O before the addition of 2-MBI. Otherwise, the initial 2-MBI adsorption onto the nitrogen-filled AgNP sample would reduce solution pH or release hydrogen gas as predicted with reactions 1−3 in Figure 7. Unfortunately, it is currently impossible to determine the thickness of the silver oxide shell for AgNPs in water. However, the fact that 2-MBI can be slowly, but continuously, adsorbed onto AgNPs in the nitrogen-filled sample during the entire 2 day experimental period suggests the possibility that multiple layers of Ag atoms near the AgNP surface were oxidized before 2-MBI addition.

Continuous 2-MBI adsorption has also been observed with planar silver foil in water, which is in sharp contrast to 2-MBI adsorption on the gold foil (Figure 9). 2-MBI reached saturation adsorption on gold foil after ∼10 h of sample incubation. However, continuous 2-MBI adsorption onto silver foil was observed during the entire 2 day experimental period until complete 2-MBI consumption occurred. The nominal 2-MBI packing densities on the gold and silver foils in Figure 9 were calculated on the assumption that foils were perfectly smooth and all the 2-MBI adsorbed onto the foils remained attached to the metal surfaces. The nominal saturation 2-MBI packing density observed on the gold foil is ∼40% higher than the monolayer 2-MBI packing density (570 pmol/cm^2) reported for the AuNPs.[28,30] One most likely reason for this discrepancy is the gold foil surface roughness. The actual surface area of the gold foil should be inevitably larger than that used for calculation. Consequently, the actual 2-MBI packing density on gold foil should be smaller than the nominal 2-MBI saturation calculated in Figure 9. On the other hand, if we assume that surface roughness of the silver foil is similar as that of the gold foil, the only reasonable explanation for the exceedingly high 2-MBI packing density on the silver foil is multilayer 2-MBI adsorption onto the silver foil. This explanation is consistent with aforementioned experimental observation of the multilayer 2-MBI adsorption onto AgNPs in water. Presumably the mechanism for the continuous 2-MBI adsorption onto the silver foil in water is the same as that proposed in this work for the aromatic OT adsorptions onto AgNPs in water.

CONCLUSIONS

In summary, OT adsorption experiments onto AgNPs and Au@Ag provide unequivocal evidence that the aromatic OTs probed in this study can continuously react with AgNPs in water until complete OT or AgNP consumption has occurred. The initial OT adsorption onto the AgNPs in water proceeds through OT reaction with Ag_2O on AgNP surfaces. Environmental oxygen is involved in this continuous reactive OT adsorption onto the AgNPs. This reaction of core Ag atoms

dx.doi.org/10.1021/jp4090102 | J. Phys. Chem. C 2013, 117, 27146−27154

with OT in the presence of oxygen may be depicted with the equation $2Ag + 2RS{-}H + O_2 = 2RS{-}Ag + H_2O$. This reaction scheme is consistent with our observation that the OT adsorption onto the AgNP does not involve hydrogen gas generation or the release of protons. The RS−Ag complexes formed can remain on the AgNP surfaces, converting these particles into core−shell structures. The shell thicknesses increase with increased OT adsorption. This work, in combination with our recent report of OTs interaction with the AuNPs,[11] highlights the striking difference in the fundamental mechanisms of the OT interaction with AuNPs versus AgNPs.

■ ASSOCIATED CONTENT

Supporting Information

Computational simulation, UV−vis spectra, and TEM images of as-synthesized AgNPs, commercial 50 nm AgNPs, and Au@Ag nanoparticle, DLS measurement of AgNP/*p*-BDT, stability of 2-MBI, *p*-MBT, and *p*-BDT in water, and correlation between the amount of H^+ released and amount of OT reacted. This material is available free of charge via the Internet at http://pubs.acs.org.

■ AUTHOR INFORMATION

Corresponding Author

*E-mail: Dongmao@chemistry.msstate.edu (D.Z.).

Notes

The authors declare no competing financial interest.

■ ACKNOWLEDGMENTS

This work was supported by the NSF CAREER Award (CHE 1151057) and NSF fund (EPS-0903787) provided to D.Z. S.Z. is grateful for the support from ONR, NSF, and ACS/PRF. The TEM work was supported by the National Science Foundation (MRI-1126743). We gratefully acknowledge the TEM work at Institute for Imaging and Analytical Technologies (I2AT) at Mississippi State University.

■ REFERENCES

(1) Singh, P.; Lamanna, G.; Ménard-Moyon, C.; Toma, F. M.; Magnano, E.; Bondino, F.; Prato, M.; Verma, S.; Bianco, A. Formation of Efficient Catalytic Silver Nanoparticles on Carbon Nanotubes by Adenine Functionalization. *Angew. Chem., Int. Ed.* **2011**, *50*, 9893−9897.

(2) Chen, Y.; Munechika, K.; Ginger, D. S. Dependence of Fluorescence Intensity on the Spectral Overlap between Fluorophores and Plasmon Resonant Single Silver Nanoparticles. *Nano Lett.* **2007**, *7*, 690−696.

(3) Lal, S.; Grady, N. K.; Kundu, J.; Levin, C. S.; Lassiter, J. B.; Halas, N. J. Tailoring Plasmonic Substrates for Surface Enhanced Spectroscopies. *Chem. Soc. Rev.* **2008**, *37*, 898−911.

(4) Graham, D.; Faulds, K.; Smith, W. E. Biosensing Using Silver Nanoparticles and Surface Enhanced Resonance Raman Scattering. *Chem. Commun.* **2006**, *0*, 4363−4371.

(5) Xiu, Z.-m.; Zhang, Q.-b.; Puppala, H. L.; Colvin, V. L.; Alvarez, P. J. J. Negligible Particle-Specific Antibacterial Activity of Silver Nanoparticles. *Nano Lett.* **2012**, *12*, 4271−4275.

(6) Andreou, C.; Hoonejani, M. R.; Barmi, M. R.; Moskovits, M.; Meinhart, C. D. Rapid Detection of Drugs of Abuse in Saliva Using Surface Enhanced Raman Spectroscopy and Microfluidics. *ACS Nano* **2013**, *7*, 7157−7164.

(7) Li, J.-F.; Huang, Y.-F.; Duan, S.; Pang, R.; Wu, D.-Y.; Ren, B.; Xu, X.; Tian, Z.-Q. SERS and DFT Study of Water on Metal Cathodes of Silver, Gold and Platinum Nanoparticles. *Phys. Chem. Chem. Phys.* **2010**, *12*, 2493−2502.

(8) Lee, K. J.; Nallathamby, P. D.; Browning, L. M.; Osgood, C. J.; Xu, X.-H. N. In Vivo Imaging of Transport and Biocompatibility of Single Silver Nanoparticles in Early Development of Zebrafish Embryos. *ACS Nano* **2007**, *1*, 133−143.

(9) Graham, D.; Thompson, D. G.; Smith, W. E.; Faulds, K. Control of Enhanced Raman Scattering Using a DNA-Based Assembly Process of Dye-Coded Nanoparticles. *Nat. Nanotechnol.* **2008**, *3*, 548−551.

(10) Nie, Z.; Petukhova, A.; Kumacheva, E. Properties and Emerging Applications of Self-Assembled Structures Made from Inorganic Nanoparticles. *Nat. Nanotechnol.* **2010**, *5*, 15−25.

(11) Ansar, S. M.; Perera, G. S.; Jiang, D.; Holler, R. A.; Zhang, D. Organothiols Self-Assembled onto Gold: Evidence for Deprotonation of the Sulfur-Bound Hydrogen and Charge Transfer from Thiolate. *J. Phys. Chem. C* **2013**, *117*, 8793−8798.

(12) Love, J. C.; Estroff, L. A.; Kriebel, J. K.; Nuzzo, R. G.; Whitesides, G. M. Self-Assembled Monolayers of Thiolates on Metals as a Form of Nanotechnology. *Chem. Rev.* **2005**, *105*, 1103−1170.

(13) Matthiesen, J. E.; Jose, D.; Sorensen, C. M.; Klabunde, K. J. Loss of Hydrogen upon Exposure of Thiol to Gold Clusters at Low Temperature. *J. Am. Chem. Soc.* **2012**, *134*, 9376−9379.

(14) Laibinis, P. E.; Whitesides, G. M.; Allara, D. L.; Tao, Y. T.; Parikh, A. N.; Nuzzo, R. G. Comparison of the Structures and Wetting Properties of Self-Assembled Monolayers of n-Alkanethiols on the Coinage Metal Surfaces, Copper, Silver, and Gold. *J. Am. Chem. Soc.* **1991**, *113*, 7152−7167.

(15) Hu, L.; Zhang, Z.; Zhang, M.; Efremov, M. Y.; Olson, E. A.; de la Rama, L. P.; Kummamuru, R. K.; Allen, L. H. Self-Assembly and Ripening of Polymeric Silver−Alkanethiolate Crystals on Inert Surfaces. *Langmuir* **2009**, *25*, 9585−9595.

(16) Ulman, A. Formation and Structure of Self-Assembled Monolayers. *Chem. Rev.* **1996**, *96*, 1533−1554.

(17) Bryant, M. A.; Pemberton, J. E. Surface Raman Scattering of Self-Assembled Monolayers Formed from 1-Alkanethiols at Silver [Electrodes]. *J. Am. Chem. Soc.* **1991**, *113*, 3629−3637.

(18) Fenter, P.; Eisenberger, P.; Li, J.; Camillone, N.; Bernasek, S.; Scoles, G.; Ramanarayanan, T. A.; Liang, K. S. Structure of Octadecyl Thiol Self-Assembled on the Silver(111) Surface: An Incommensurate Monolayer. *Langmuir* **1991**, *7*, 2013−2016.

(19) Stewart, A.; Zheng, S.; McCourt, M. R.; Bell, S. E. J. Controlling Assembly of Mixed Thiol Monolayers on Silver Nanoparticles to Tune Their Surface Properties. *ACS Nano* **2012**, *6*, 3718−3726.

(20) Gan, W.; Xu, B.; Dai, H.-L. Activation of Thiols at a Silver Nanoparticle Surface. *Angew. Chem., Int. Ed.* **2011**, *50*, 6622−6625.

(21) Cho, S. H.; Han, H. S.; Jang, D.-J.; Kim, K.; Kim, M. S. Raman Spectroscopic Study of 1,4-Benzenedithiol Adsorbed on Silver. *J. Phys. Chem.* **1995**, *99*, 10594−10599.

(22) Han, S. W.; Lee, S. J.; Kim, K. Self-Assembled Monolayers of Aromatic Thiol and Selenol on Silver: Comparative Study of Adsorptivity and Stability. *Langmuir* **2001**, *17*, 6981−6987.

(23) Ansar, S. M.; Li, X.; Zou, S.; Zhang, D. Quantitative Comparison of Raman Activities, SERS Activities, and SERS Enhancement Factors of Organothiols: Implication to Chemical Enhancement. *J. Phys. Chem. Lett.* **2012**, *3*, 560−565.

(24) Cho, S. H.; Han, H. S.; Jang, D.-J.; Kim, K.; Kim, M. S. Raman Spectroscopic Study of 1,4-Benzenedithiol Adsorbed on Silver. *J. Phys. Chem.* **1995**, *99*, 10594−10599.

(25) McLellan, J. M.; Li, Z.-Y.; Siekkinen, A. R.; Xia, Y. The SERS Activity of a Supported Ag Nanocube Strongly Depends on Its Orientation Relative to Laser Polarization. *Nano Lett.* **2007**, *7*, 1013−1017.

(26) Rycenga, M.; Kim, M. H.; Camargo, P. H. C.; Cobley, C.; Li, Z.-Y.; Xia, Y. Surface-Enhanced Raman Scattering: Comparison of Three Different Molecules on Single-Crystal Nanocubes and Nanospheres of Silver. *J. Phys. Chem. A* **2009**, *113*, 3932−3939.

(27) Maitani, M. M.; Ohlberg, D. A. A.; Li, Z.; Allara, D. L.; Stewart, D. R.; Williams, R. S. Study of SERS Chemical Enhancement Factors Using Buffer Layer Assisted Growth of Metal Nanoparticles on Self-Assembled Monolayers. *J. Am. Chem. Soc.* **2009**, *131*, 6310−6311.

(28) Ansar, S. M.; Haputhanthri, R.; Edmonds, B.; Liu, D.; Yu, L.; Sygula, A.; Zhang, D. Determination of the Binding Affinity, Packing, and Conformation of Thiolate and Thione Ligands on Gold Nanoparticles. *J. Phys. Chem. C* **2011**, *115*, 653−660.
(29) Osberg, K. D.; Rycenga, M.; Harris, N.; Schmucker, A. L.; Langille, M. R.; Schatz, G. C.; Mirkin, C. A. Dispersible Gold Nanorod Dimers with Sub-5 nm Gaps as Local Amplifiers for Surface-Enhanced Raman Scattering. *Nano Lett.* **2012**, *12*, 3828−3832.
(30) Zhang, D.; Ansar, S. M. Ratiometric Surface Enhanced Raman Quantification of Ligand Adsorption onto a Gold Nanoparticle. *Anal. Chem.* **2010**, *82*, 5910−5914.
(31) Zhang, D.; Xie, Y.; Mrozek, M. F.; Ortiz, C.; Davisson, V. J.; Ben-Amotz, D. Raman Detection of Proteomic Analytes. *Anal. Chem.* **2003**, *75*, 5703−5709.
(32) Lee, P. C.; Meisel, D. Adsorption and Surface-Enhanced Raman of Dyes on Silver and Gold Sols. *J. Phys. Chem.* **1982**, *86*, 3391−3395.
(33) Jana, N. R.; Gearheart, L.; Murphy, C. J. Seeding Growth for Size Control of 5−40 nm Diameter Gold Nanoparticles. *Langmuir* **2001**, *17*, 6782−6786.
(34) Mie, G. Betirage zur optik Truber Medien, spexiell Killoidaler Metalasungen. *Ann. Phys.* **1908**, *25*, 377.
(35) Zou, S. Electromagnetic Wave Propagation in a Multilayer Silver Particle. *Chem. Phys. Lett.* **2008**, *454*, 289−293.
(36) Palik, E. D. *Handbook of Optical Constants of Solids*; Academic Press: New York, 1985.
(37) Horn, E.; Kurahashi, M. The Crystal Structure Determination of 1,4-Benzenedithiol from X-Ray Powder Diffraction Data. *X-sen Bunseki no Shinpo* **1996**, *27*, 129−38.
(38) Gadogbe, M.; Ansar, S.; He, G.; Collier, W.; Rodriguez, J.; Liu, D.; Chu, I. W.; Zhang, D. Determination of Colloidal Gold Nanoparticle Surface Areas, Concentrations, and Sizes through Quantitative Ligand Adsorption. *Anal. Bioanal. Chem.* **2012**, *405*, 1−10.
(39) Dance, I. G.; Fisher, K. J.; Banda, R. M. H.; Scudder, M. L. Layered Structure of Crystalline Compounds Silver Thiolates (AgSR). *Inorg. Chem.* **1991**, *30*, 183−187.
(40) Baena, M. J.; Espinet, P.; Lequerica, M. C.; Levelut, A. M. Mesogenic Behavior of Silver Thiolates with Layered Structure in the Solid State: Covalent Soaps. *J. Am. Chem. Soc.* **1992**, *114*, 4182−4185.
(41) Li, X.; Lenhart, J. J.; Walker, H. W. Dissolution-Accompanied Aggregation Kinetics of Silver Nanoparticles. *Langmuir* **2010**, *26*, 16690−16698.
(42) Yin, Y.; Li, Z.-Y.; Zhong, Z.; Gates, B.; Xia, Y.; Venkateswaran, S. Synthesis and Characterization of Stable Aqueous Dispersions of Silver Nanoparticles through the Tollens Process. *J. Mater. Chem.* **2002**, *12*, 522−527.
(43) Chen, M.; Wang, L.-Y.; Han, J.-T.; Zhang, J.-Y.; Li, Z.-Y.; Qian, D.-J. Preparation and Study of Polyacryamide-Stabilized Silver Nanoparticles through a One-Pot Process. *J. Phys. Chem. B* **2006**, *110*, 11224−11231.
(44) Henglein, A. Colloidal Silver Nanoparticles: Photochemical Preparation and Interaction with O_2, CCl_4, and Some Metal Ions. *Chem. Mater.* **1998**, *10*, 444−450.
(45) Allum, K. G.; Creighton, J. A.; Green, J. H. S.; Minkoff, G. J.; Prince, L. J. S. The Vibrational Spectra of Some Dialkyl and Diaryl Disulphides and of Di-n-butyl Diselenide. *Spectrochim. Acta, Part A* **1968**, *24*, 927−941.
(46) Green, J. H. S. Vibrational spectra of benzene derivatives—IV. Methylphenyl Sulphide, Diphenyl Sulphide, Diphenyl Disulphide and Diphenyl Sulphoxide. *Spectrochim. Acta, Part A* **1968**, *24*, 1627−1637.
(47) Lim, J. K.; Kwon, O.; Joo, S.-W. Interfacial Structure of 1,3-Benzenedithiol and 1,3-Benzenedimethanethiol on Silver Surfaces: Surface-Enhanced Raman Scattering Study and Theoretical Calculations. *J. Phys. Chem. C* **2008**, *112*, 6816−6821.